Lab on a Chip

Accepted Manuscript

RSC Publishing

www.rsc.org/loc

Registered Charity Number 207890

Separation of motile bacteria using drift velocity in a microchannel

Takuji Ishikawa[1,2,*], Tatsuya Shioiri[1], Keiko Numayama-Tsuruta[2], Hironori Ueno[3], Yohsuke Imai[1] and Takami Yamaguchi[2]

[1] Dept. Bioengineering and Robotics, Graduate School of Engineering, Tohoku University, 6-6-01 Aoba, Aramaki, Aoba-ku, Sendai 980-8579, Japan

[2] Dept. Biomedical Engineering, Graduate School of Biomedical Engineering, Tohoku University, 6-6-01 Aoba, Aramaki, Aoba-ku, Sendai 980-8579, Japan

[3] Molecular function and life science, Aichi University of Education, 1 Hirosawa, Igaya-cho, Kariya, Aichi 448-8542, Japan

[*]Corresponding author:
Takuji Ishikawa
Department of Bioengineering and Robotics,
Graduate School of Engineering, Tohoku University
6-6-01, Aoba, Aramaki, Aoba-ku, Sendai 980-8579, Japan
Tel: +81-22-795-4009
Fax: +81-22-795-6959
E-mail: ishikawa@pfsl.mech.tohoku.ac.jp

Abstract

Separation of certain bacteria from liquids is important in the food, water quality management, bioengineering, and pharmaceutical industries. In this study, we developed a microfluidic device for the hydrodynamic separation of motile bacteria (*Escherichia coli*) using drift velocity. We first investigated drift tendencies of bacteria, and found that cells tended to move in a spanwise direction with similar velocities regardless of the flow rate. When the drift distance was small compared to the wetted perimeter of the cross section, the cells were not separated efficiently. We then investigated the drift phenomenon in more detail using a numerical simulation. Interestingly, the drift phenomenon was observed even without a wall boundary, indicating that drift was caused mainly by the interaction of moving cells with the background shear flow. Finally, we developed a microfluidic device to separate motile bacteria from tracer particles or less motile cells. By decreasing the channel height, the device could successfully separate motile bacteria from other particles or cells with a separation efficiency of about 40%. Connecting microchannels in a series was also found to be effective, which achieved the separation efficiency of about 60%. The knowledge obtained in this study will facilitate development of other microfluidics devices for use with bacteria.

1. Introduction

Detection of bacteria is critical to the food industry, water quality management, bioengineering and medicine. Many bacteria-detection methods have been proposed, such as nucleic acid staining [1,2] and a microcolony technique [3,4]. Recently, micro-device methods for the detection or separation of bacteria have been proposed, including dielectrophoresis [5,6], and magnetic force [7-10]. However, the use of electric or magnetic fields sometimes requires complex preparation procedures and considerable space to house the separation apparatus.

To overcome these problems, microfluidic devices for hydrodynamic separation of bacteria have been developed. Wu *et al*. [11] utilized hydrodynamic inertial forces to separate *Escherichia coli* (*E. coli*) from blood cells, in which the difference in size between the bacteria and the blood cells was the principal separation mechanism. Galajda *et al*. [12] developed a unique separation method based on the formation of a concentration gradient in *E. coli* colonies by utilizing the difference between entry and reflection angles when bacteria interact with a solid wall. Hulme *et al*. [13] reported ratchets and sorters for *E. coli* fractionation by length, and successfully isolated shorter populations of bacteria. Hydrodynamic separation was also performed for sperm cells [14,15], in which the ability of motile sperm to cross streamlines in a laminar flow was utilized.

E. coli bacteria are known to move in a circular pattern when located near a solid wall in a fluid otherwise at rest; this movement has been explained using hydrodynamic forces [16,17]. Chiral objects, such as helical flagella, drift perpendicularly to the shear plane [18]. When both wall effects and shear flow effects were combined, most *E. coli* cells near a wall tended to move in a spanwise direction, as reported by Hill *et al*. [19]. In this study, we

utilized this near-wall drift velocity and developed a micro-fluidic device to separate motile bacteria.

We first investigated bacterial drift tendencies using a simple microchannel, as described in section three. Although the basic mechanism of bacterial near-wall drift was explained briefly by Hill *et al*. [19], further investigation was required to fully understand this phenomenon and to utilize it in development of a micro-fluidic device. We thus developed a computational model for *E. coli* using a boundary element method, as described in section four. Last, we developed a microfluidic device for the separation of motile bacteria from tracer particles or less-motile bacteria, as described in sections 5 and 6.

2. Materials and Methods

2.1 Experimental setup and microchannels

The experimental apparatus consisted primarily of an inverted microscope (IX71, Olympus, Tokyo, Japan) and a high-speed camera (Phantom v7.1; Vision Research, Wayne, NJ). A microfluidic device was placed on the stage, and the sample was injected using syringe pumps (Fusion 200; Chemyx Inc., Stanford, TX). Images of bacteria and tracer particles were obtained with a high-speed camera and recorded using a desktop PC.

Schematic representations of two types of microchannels are shown in Fig. 1. White arrows indicate the behavior of motile bacteria. Bacteria near the bottom wall drift to the right until they collide to the side wall. When they reach the side wall, they drift to the top wall. Cells near the top wall then drift to the left and collide to the partition on the top wall. Bacteria at the partition drift towards the bottom wall, and they do not return to the left side of the channel. This is how motile cells accumulate on the right side.

Microchannel A [Fig.1(a)] was used for observing drift phenomena of bacteria, and microchannel B [Fig.1(b)] was used to separate bacteria from other particles or cells. The microchannels had two inlets and two outlets. The main channel of A [Fig.1(a)] was 500 μm wide, 16 mm long, and 50 or 150 μm high. The main channel of B [Fig.1(b)] was 450 μm wide and 16 mm long. The minimum height of the channel was 15 μm, and the maximum height H was 30 or 115 μm.

The microchannels were fabricated by standard soft lithography using a protocol similar to that described previously [20,21]. Briefly, a two-layer mold for the channel was fabricated on a silicon wafer with negative photoresist (SU-8 3050; Kayaku MicroChem, Tokyo, Japan). Polydimethylsiloxane (PDMS) (Silpot 184; Dow Corning, Midland, MI) was prepared by mixing the base compound and curing agent at a weight ratio of 10:1. After removing bubbles created during mixing, the mixture was poured on the master mold and cured by baking for about 30 min at 90°C. The PDMS was peeled from the master, and the fluidic ports used as the inlet and the outlets were created with a punch. To prevent fluid leakage from the gap between the PDMS and glass slide, an oxygen plasma treatment was applied to irreversibly bind the PDMS and glass.

2.2 Materials

Escherichia coli, which has a cell body of about 1 μm in diameter and 2 μm in length, was used as the model bacterial species. Three kinds of *E. coli* were used in this study: (i) the wild-type strain MG1655 with high motility, (ii) MG1655 without motility, and (iii) the labeled wild-type strain JK109 with low motility.

The protocol for culturing strain MG1655 was similar to that described previously

[16,22]. The cells were grown for 12 h in tryptone broth (TB) maintained at 37°C using a rotary shaker (160 rpm). Saturated cell culture (50 μL) was diluted in 5 mL of TB, and maintained at 25°C without shaking for 10 h. The cultured bacteria, designated motile MG1655, were highly motile with a swimming velocity of about 20 μm/s. To prepare bacteria without motility, designated non-motile MG1655, we added CCCP (carbonyl cyanide *m*-chlorophenylhydrazone), which stops flagella movement, to motile MG1655 at a concentration of 20μM.

To prepare the less motile *E. coli* strain, designated JK109, we used wild-type strain JK109 carrying the fluorescent protein mOrange and an ampicillin-resistance protein. The recombinant DNA work was carried out by Tohoku University Center for Gene Research. The cells were grown for 12 h in lysogeny broth (LB) culture fluid [tryptone 1% (w/v), yeast extract 0.5% (w/v) and NaCl 0.5% (w/v)] maintained at 37°C using a rotary shaker (180 rpm). Saturated cell culture (50 μL) was diluted in 5 mL of LB, and ampicillin (250 μg) was added. The mixture was maintained at 27°C using a rotary shaker (180 rpm) for 5 h, then isopropyl b-D-1-thiogalactopyranoside (IPTG, 500 μg) was added to induce production of the fluorescent protein. Finally, the culture was maintained at 27°C using a rotary shaker (180 rpm) for 5 h. The cells were less motile, as evidenced by a swimming velocity of ~3 μm/s.

2.3 Experimental procedures

Microchannels A and B had two inlets and two outlets. As described in section three, a cultures of motile [motile MG1655] or non-motile [non-motile MG1655] cells with absorbance at 600 nm (OD600) of 0.8 (about 6.4×10^8 cells/mL) were introduced into microchannel A via the left inlet, and TB was introduced via the right inlet. We note that the

number density of cells was about 100 times less than that used in our former study [22], thus the effect of cell-cell interactions could be neglected. As described in section five, two kinds of culture fluid were introduced into microchannel B via the left inlet: (a) a culture of motile cells [motile MG1655] with an OD600 of 0.2 (about 1.6×10^8 cells/mL), including 1-μm diameter fluorescent tracer particles (FluoSphere, Molecular Probes, USA) at a concentration of 5×10^7/mL, and (b) cultures of motile cells [motile MG1655] and less motile cells [JK109], both with an OD600 of 0.2. In this case, LB was introduced via the right inlet. The flow rate Q at each inlet and outlet was controlled using syringe pumps (Fusion 200; Chemyx Inc., Stanford, TX). The detailed flow rate conditions are explained in each section.

The swimming motions of individual cells were recorded using a high-speed camera. The recorded images were evaluated with a manual tracking plug-in (MTrackJ) for the ImageJ software (NIH, Bethesda, MD, USA). With this software, the position and the velocity of a selected bacterium could be obtained using successive images.

The cell separation efficiency was defined as the ratio of cells collected from the right outlet to the total cells collected from both outlets. The number of collected cells per unit time was estimated by multiplying the flow rate by the cell density. For microchannel A, the cell density was evaluated using a bacterial counter (Sunlead Glass Corp., Saitama, Japan). For microchannel B, the cell density was evaluated by counting cells in the observation area of each outlet (cf. Fig. 1(b), in which the channel height is 15 μm) using the ImageJ software.

2.4 Numerical methods

To clarify the mechanism of drift, we performed a computational analysis. The details of the numerical methods have been reported previously [16]. Briefly, the bacterium was

modeled as an ellipsoid (2-μm long axis and 1-μm short axis) with a single flagellum (length of 7 μm), as shown in Fig. 5. The flagellum was assumed to rotate rigidly with constant angular velocity ω relative to the cell body. The bacterium was assumed to be force-free and torque-free.

A boundary element method (BEM) was used to assess the hydrodynamics in the Stokes flow regime. A half-space Green function [23] was introduced to express the effect of a solid wall. The cell body was discretized with 320 triangular elements, and the flagellum was modeled as a series of pentagonal cylinders whose surface was composed of 360 triangular elements. Integration in the boundary integral equation was performed on a triangular element using 28-point Gaussian polynomials. The singularity in the integration was solved analytically. The time marching was performed using the fourth-order Runge–Kutta method. The accuracy of this numerical method was verified by comparison with the experimental results for a solitary *E. coli* swimming near a wall [16].

3. Observation of the Drift Phenomenon using Microchannel A

In this section, the motion of motile [motile MG1655] and non-motile [non-motile MG1655] bacteria were observed in microchannel A. The flow rates at the left and right inlets and the left and right outlets were the same throughout this section. The total flow rate in the main channels was varied in the range 1.2–25 μL/min.

Figure 2(a) shows the distribution of motile bacteria near the entrance of the main channel. Cells existed in the left region only, because cell suspension was introduced via the left inlet, whereas TB was introduced via the right inlet. A similar tendency was also observed for the non-motile cells. Near the exit of the main channel, however, we observed a

clear difference between the motile and non-motile cells. In the case of motile cells [cf. Fig. 2(b)], cells spread in a spanwise direction and existed along the entire width of the region. In the case of non-motile cells [cf. Fig. 2(c)], on the other hand, the cells remained on the left side near the exit. Thus, drift was caused mainly by bacterial motility.

We then measured the separation efficiency, defined as the ratio of cells collected from the right outlet to the total cells collected from both outlets. The results at various flow rates are plotted in Fig. 3. Motile cells were separated with an efficiency of about 17%, when the flow rate was 1.2 μL/min. The efficiency decreased as the flow rate was increased. When the flow rate was higher than 12 μL/min, no differences in efficiency between the motile and the non-motile cells were evident. The separation efficiency of non-motile cells was not zero, because the cells spread due to Brownian motion. These results indicated that flow rate is one of the most important parameters for achieving high separation efficiency.

To understand the influence of flow rate on the separation efficiency, we measured the drift of individual bacteria. Figures 4(a) and (b) show the velocities of motile bacteria in the vicinity of the wall. As shown in Fig. 4(a), the drift velocity; *i.e.*, the velocity toward the right side, was always positive, and the value was minimally affected by the flow rate. The magnitude of the drift velocity was ~20 μm/s, which is equivalent to the swimming velocity of a solitary bacterium. In contrast, the velocity in the flow direction [Fig. 4(b)] increased significantly as the flow rate was increased. The slope of this relationship was almost a linear correlation.

We further calculated the drift distance, which was defined as the product of the drift velocity [cf. Fig. 4(a)] and the drift time, where the drift time was equal to the channel length (16 mm) divided by the velocity in the flow direction [cf. Fig. 4(b)]. The results are plotted in

Fig. 4(c). The drift distance decreased as the flow rate was increased; this result is consistent with the observation that the separation efficiency decreased as the flow rate was increased. The wetted perimeter of the cross section of microchannel A was 1500 μm. For cells on the left side, the maximum drift length required to move the cells into the right region along the wall is half of the wetted perimeter, *i.e.* 750 μm, which is indicated by the broken line in Fig. 4(c). The drift distance was less than 750 μm when the flow rate was higher than 12 μL/min, and the separation efficiency was not improved by the cell motility. These results indicate that the drift distance must be sufficiently large for efficient separation of motile bacteria using the drift phenomenon. The ratio of the drift distance to the half of the wetted perimeter could be used as a dimensionless parameter to rationalize the design.

4. Numerical Simulation of the Drift Phenomenon

Next, we investigated the drift phenomenon in more detail using a numerical simulation. The computational model enabled us to consider the stability of the bacterial orientation in the channel flow and to clarify the drift mechanism.

Figure 5 shows the computational setup. A wall boundary existed at $z = 0$; x was the flow direction, and y was the lateral direction. The background flow was assumed to be simple shear flow, i.e. $\mathbf{u} = (\dot{\gamma} z, 0, 0)$ where $\dot{\gamma}$ was the shear rate. Vector **e** was the unit orientation vector of a bacterium, and θ was the angle of vector **e** from the x-axis in the x-y plane. Parameter d was the minimum distance between the wall and the cell body. Value $\dot{\gamma}$ was set at 0.1ω throughout this section. By assuming an angular velocity for *E .coli* of $\omega = 500$ rad/s, the shear rate could be derived as 50 s^{-1}. This shear rate corresponded to a flow rate of about 5 μL/min in the microchannel A experiments.

We first performed computations under simple shear flow without a wall boundary, thereby enabling verification of shear flow effects separately from wall effects. When the initial orientation of cells, $\mathbf{e}_0$, was directed toward a positive or negative direction with respect to each coordinate axis [Fig. 6(a)], most of the cells drifted in the positive *y* direction; *i.e.*, in the same (right) direction as observed in the microchannel A experiments, except that one cell initially directed toward a negative *y* direction continuously swam in a negative *y* direction. Drift was observed even without a wall boundary, although *E. coli* has been previously reported to drift only near a wall [19]. Drift is caused principally by hydrodynamic forces generated for chiral objects [18], in which rotational velocity is generated to satisfy the torque-free condition of the entire cell body.

When $\mathbf{e}_0$ was placed in the *x*-*y* plane at various initial angles θ_0, the trajectories varied as shown in Fig. 6(b). Cells with $\theta_0 = 240{-}300°$ exhibited drift in the opposite direction, whereas cells with $\theta_0 = 0{-}210°$ and $330{-}360°$ exhibited drift in the normal direction. Thus, the normal drift phenomenon was stable in a large region in the orientation space of $\mathbf{e}_0$.

We then performed computations with a wall boundary with an initial distance $d_0 = 4.5a$, where *a* was the half-body length of *E. coli*. The initial orientation vector $\mathbf{e}_0$ was placed in the *x*-*y* plane at various initial angles θ_0. The cell trajectories are plotted in Fig. 7(a). Cells with $\theta_0 = 240{-}300°$ exhibited drift in the opposite direction, whereas cells with $\theta_0 = 0{-}210°$ and $330{-}360°$ exhibited drift in the normal direction, which is the same tendency as shown in Fig. 6(b). These results suggest that the mechanisms of bacterial drift in the presence of a wall are similar to those in the absence of a wall; *i.e.*, interactions between cell swimming and background shear flow.

Figure 7(b) shows the *y* component of the orientation vector e_y as a function of time *t*. We

observed that e_y of the drifted cells eventually converged to a value of about 0.93, thereby indicating that the orientation of these cells was nearly towards the positive *y* direction. This result explains why the drift velocity shown in Fig. 4(a) was equivalent to the swimming velocity of *E. coli*. Although cells exhibited drift regardless of the distance from the wall, drift distance was strongly influenced by the velocity in the flow direction. The velocity in the flow direction increased as the distance from the wall increased, so the drift phenomenon was pronounced for cells near a wall. These results clarified the drift mechanism and the importance of the wall for hydrodynamic separation of bacteria.

5. Separation of Motile Bacteria using Microchannel B

The knowledge obtained in the previous sections was used to develop microchannel B for separating motile bacteria. To prohibit non-motile cells from exiting via the right outlet, we modified the flow rate conditions at the inlets and outlets. The flow rate at the left inlet was maintained at 0.3 μL/min, whereas that at the right inlet was maintained at 0.6 μL/min. The flow rate was 0.45 μL/min at both outlets. These flow conditions prevent non-motile particles from exiting via the right outlet, because the streamline that divides the flow from the left and right inlets drifts to the left side and runs into the left outlet.

We first performed experiments using a culture of motile cells [motile MG1655] that included 1 μm diameter fluorescent tracer particles. The separation efficiencies at channel heights *H* of 30 and 115 μm are shown in Fig. 8. The fluorescent tracer particles did not exit via the right outlet, indicating that the given flow rate conditions efficiently prevented Brownian diffusion of tracers. The separation efficiency at H = 30 μm was ~40%, although that at H = 115 μm was only ~10%. Higher separation efficiency was achieved when the cells

remained near the walls where the velocity in the flow direction was low. When cells remain far away from the wall, on the other hand, the velocity in the flow direction becomes significantly larger than the drift velocity. Such cells do not have sufficiently long time to drift. Low channel heights were thus more efficient for cell separation.

To observe the influence of partitions on the top wall, the culture fluid inlet was inverted from the left to the right. In this inverted flow condition, a culture of motile cells [motile MG1655] was introduced via the right inlet at a rate of 0.3 μL/min, and LB was introduced via the left inlet at a rate of 0.6 μL/min (H = 30 μm). In this scenario, if the partitions on the top wall have no influence, the separation efficiency (here defined by the ratio of cells collected from the left outlet to total cells) should be the same as that observed under the normal conditions. However, as shown in Fig. 8, the separation efficiency decreased from 40% to 7% when the inlet flow was inverted (H = 30 μm). These results clearly indicate that the partitions were important for achieving high separation efficiency. *E. coli* cells tended to swim parallel to the wall, so the partitions prevented cells from swimming continuously in the same direction. Partitions on the top wall also encouraged cell movement toward the bottom wall on average. This directional modification of the cell movement is the reason that the existence of partitions improved the separation efficiency.

To determine if the developed microchannel could be utilized to separate cells based on their motility, we evaluated cultures including both motile cells [motile MG1655] and less-motile cells [JK109]. The culture fluid was introduced via the left inlet at a rate of 0.3 μL/min, and LB was introduced via the right inlet at a rate of 0.6 μL/min. A fluorescence image near the outlet is shown in Fig. 9(a), in which labeled less-motile bacteria (JK109) can be seen near the left outlet. In the bright-field images [Fig. 9(b) and (c)], bacteria are evident

even at the right outlet. Because those cells at the right outlet were not labeled, only motile bacteria (MG1655) exited at the right. The separation efficiency of motile bacteria was about 35% in this case (standard deviation in three independent experiments was about 4%). We could not find any labeled cells at the right outlet throughout the study, which indicates the purity of the motile cells was almost 100%. Such a high purity could be achieved by controlling the inlet flow rate ratio as 1 : 2 while keeping the outlet flow rate ratio as 1.5 : 1.5. Thus, the present device enabled separation of bacteria based on their motility.

6. Separation by a Series of Three Microchannels

In order to improve the separation efficiency, connecting microchannels in a series might be effective. We thus designed a series of three microchannels, similar to microchannel B, as shown in Fig.10. The device had one inlet of a bacterial suspension, three inlets of buffer fluid and four outlets. The main channel was 3mm wide and 16 mm long. The minimum height was 15 μm, and the maximum height was 30 μm.

A culture of motile cells [motile MG1655] with an OD600 of 0.2, including 1-μm diameter fluorescent tracer particles at a concentration of 5×10^7/mL, was introduced via the inlet of a bacterial suspension with the flow rate of 1.5 μL/min. LB was introduced via three inlets of buffer fluid, where the flow rate of each inlet was maintained at 4.5 μL/min. Atmospheric pressure was applied at the four outlets. In order to keep the buffer flow rate three times larger than the sample flow rate in all three microchannels, we adjusted the pressure loss at the four outlets. The pressure loss was calculated as explained in Yamada & Seki [24], and controlled by adjusting the channel length between the main channels and the outlets.

The cell separation efficiency was defined as the ratio of cells collected from outlets 1, 2 and 3 (cf. Fig.10) to the total cells collected from all four outlets. The cell density was evaluated using a bacterial counter. The results showed that the separation efficiency of the series of three microchannels was about 60% (standard deviation in three independent experiments was about 9%). The tracer particles, introduced via the inlet of a bacterial suspension, remained about 92% at outlet 4 (standard deviation in three independent experiments was about 2%). Thus, most of inert particles remained at outlet 4 while about 60% of motile cells were removed. These results indicate that the connection of microchannels in a series is an effective strategy to increase the separation efficiency.

7. Conclusions

In this study, we developed a microfluidic device to separate motile bacteria (*E. coli*) using the near-wall drift velocity. We first investigated bacterial drift tendencies using microchannel A. Cells tended to swim in a spanwise direction at similar velocities regardless of the flow rate. We proposed drift distance as an indicator of separation efficiency. When the drift distance was small compared to the wetted perimeter of the cross section, the cells were not separated efficiently.

We then investigated the drift phenomenon in more detail using a numerical simulation. The drift phenomenon appeared even without a wall boundary, although the drift of *E. coli* has been previously reported to occur only near a wall [19]. The stability of the drift in the orientation space of $\mathbf{e}_0$ did not significantly differ with or without a wall, which indicated that the bacteria drift was mainly caused by the interaction of cell swimming and the background shear flow. The results also suggested the importance of the wall when utilizing drift to

separate bacteria, because cell drift is pronounced near a wall where the velocity in the flow direction is small.

The knowledge obtained in this study was then used to develop microchannel B for separation of motile bacteria. When channel height H = 30 μm, the separation efficiency was ~40%. The separation efficiency was improved by reducing the channel height. Partitions on the top wall were important for improving the separation efficiency. Microchannel B was also used to separate cells based on their motility. The results clearly indicated that the developed microfluidic device successfully separated bacteria based on their motility.

Last, we designed a series of three microchannels in order to improve the separation efficiency. The results showed that the separation efficiency was improved up to about 60%, while most of inert particles were remained. Thus, the connection of microchannels in a series is an effective strategy to increase the separation efficiency. The knowledge obtained in this study will facilitate development of other microfluidic devices for use in conjunction with bacteria.

Acknowledgement

This study was supported by Grants-in-Aid for Scientific Research (S), Specially Promoted Research, and the NEXT program of JSPS. We also acknowledge NBRP-E.coli at NIG for supplying the MG1655 clone.

References

[1] Nakajima, K., Nonaka, K., Yamamoto, K., Yamaguchi, N., Tani, K. and Nasu, M., Rapid monitoring of microbial contamination on herbal medicines by fluorescent staining

method, *Lett. Appl. Microbial.*, **40**, pp. 128-132, (2005)

[2] Li, W. K. W., Jellett, J. F. and Dickie, P. M., Flow cytometric analysis of marine bacteria stained with TOTO or TO-PRO, *Limnol. Oceanogr*., **40**, pp. 1485-1495, (1995)

[3] Hesselsøe, M., Brandt, K. K. and Sørensen, J., Quantification of ammonia oxidizing bacteria in soil using microcolony technique combined with fluorescence in situ hybridization (MCFU-FISH), *FEMS Microbiol. Ecol*., **38**, pp. 87-95, (2001)

[4] Rodrigues, U. M. and Kroll, R. G., Rapid selective enumeration of bacteria in foods using a microcolony epifluorescence microscopy technique, *J. Appl. Bacterial.*, **64**, pp. 65-78, (1988)

[5] Lapizco-Encinas, B. H., Simmons, B. A., Cummings, E. B. and Finschenko, Y., Dielectrophoretic Concentration and Separation of Live and Dead Bacteria in an Array of Insulators, *Analytical Chemistry*, **76**, pp. 1571-1579, (2004)

[6] Markx, G. H., Dyda P. A. and Pething, R., Dielectrophoretic separation of bacteria using conductivity gradient, *J. Biotechnology*, **51**, pp.175-180, (1996)

[7] Sakuma, S., Yamanishi, Y. and Arai, F., Actuation of Magnetically Driven Microtools by Focused Magnetic Field for Separation of Micro-particles, *J. Robotics Mechatronics*, 21, pp. 209-215, (2009)

[8] Yamanishi, Y., Sakuma, S., Onda, K. and Arai, F., Biocompatible Polymeric Magnetically Driven Microtool for Particle Sorting, *J. Micro Nano Mechatronics*, **4**, pp. 49-57, (2008)

[9] Shih, P.-H., Shiu, J.-T., Lin, P.-C., Lin, C.-C., Veres, T. and Chen, P., On chip sorting of bacterial cells using sugar-encapsulated magnetic nanoparticles, *J. Appl. Phys*., **103**, 07A316, (2008)

[10] Xia, N., Hunt, T. P., Mayers, B. T., Alsberg, E., Whitesides, G. N., Westervelt, R. N. and Ingber, D. E., Combined microfluidic-micromagnetic separation of living cells in continuous flow, *Biomed. Microdev.*, **8**, pp. 299-308, (2006)

[11] Wu, Z., Willing, B., Bjerketirp, J., Jansson, J. K. and Hjort, K., Softr inertial microfluidics for high throuput separation of bacteria from human blood cells, *Lab Chip*, **9**, pp. 1193-1119, (2009)

[12] Galajda, P., Keymer, J., Chakin, P. and Austin, R., A Wall of Funnels Concentrates Swimming Bacteria, *J. Bacteriology*, **189**, pp. 8704-8707, (2007)

[13] Hulme, S. E., Diluzio, W. R., Shevkoplyas, S. S., Turner, L., Mayer, M., Berg, H. C. and Whitesides, G. M., Using ratchets and sorters to fractionate motile cells of Escherichia coli by length, *Lab Chip*, **8**, pp. 1888-1895, (2008)

[14] Wu, J. M., Chung, Y., Belford, K. J., Smith, G. D., Takayama, S. and Lahann, J., A surface-modified sperm sorting device with long-term stability, *Biomed. Microdev.*, **8**, pp. 99-107, (2006)

[15] Cho, B., Schuster, T. G., Zhu, X., Chang, D., Smith, G. D. and Takayama, S., A Passively-Driven Integrated Microfluidic System for Separation of Motile Sperm, *Anal. Chem.*, **75**, pp. 1671-1675, (2003)

[16] Giacche, D., Ishikawa, T. and Yamaguchi, T., Hydrodynamic entrapment of bacteria swimming near a solid surface, *Phys. Rev. E*, **82**, 056309 (2010)

[17] Lauga, E., DiLuzio, W. R., Whitesides, G. M. and Stone, H., Swimming in Circles: Motion of Bacteria near Solid Boundaries, *Biophys. J.* **90**, 400–412, (2006)

[18] Fu, M. H. C., Powers T. R. and Stocker, R., Separation of Microscale Chiral Objects by Shear Flow, *Phys. Rev. Lett.*, **102**, 158103, (2009)

[19] Hill, J., Kalkanci, O., McMury, J. L. and Koser, H., Hydrodynamic Surface Interactions Enable Escherichia Coli to Seek Efficient Routes to Swim Upstream, *Phys. Rev. Lett*., **98**, 068101, (2007)

[20] Lima, R., Wada, S., Tanaka, S., Takeda, M., Ishikawa, T., Tsubota, K., Imai, Y. and Yamaguchi, T., In vitro blood flow in a rectangular PDMS microchannel: experimental observations using a confocal micro-PIV system, *Biomed. Microdevices*, **10**, pp.153-167, (2008)

[21] Tanaka, T., Ishikawa, T., Numayama-Tsuruta, K., Imai, Y., Ueno, H., Matsuki, N. and Yamaguchi, T., Separation of cancer cells from a red blood cell suspension using inertial force, *Lab Chip*, **12**, pp. 4336-4343, (2012)

[22] Ishikawa, T., Yoshida, N., Ueno, H., Wiedeman, M., Imai, Y. and Yamaguchi, T., Energy transport in a concentrated suspension of bacteria, *Phys. Rev. Lett.*, **107**, 028102, (2011)

[23] Blake, J. R. and Chwang, A. T., Fundamental singularities of viscous flow. Part I: The image systems in the vicinity of a stationary no-slip boundary, *J. Eng. Math.*, **8**, pp. 23–29, (1974)

[24] Yamada, M. and Seki, M., Hydrodynamic filtration for on-chip particle concentration and classification utilizing microfluidics, *Lab chip*, **5**, pp.1233-1239, (2005)

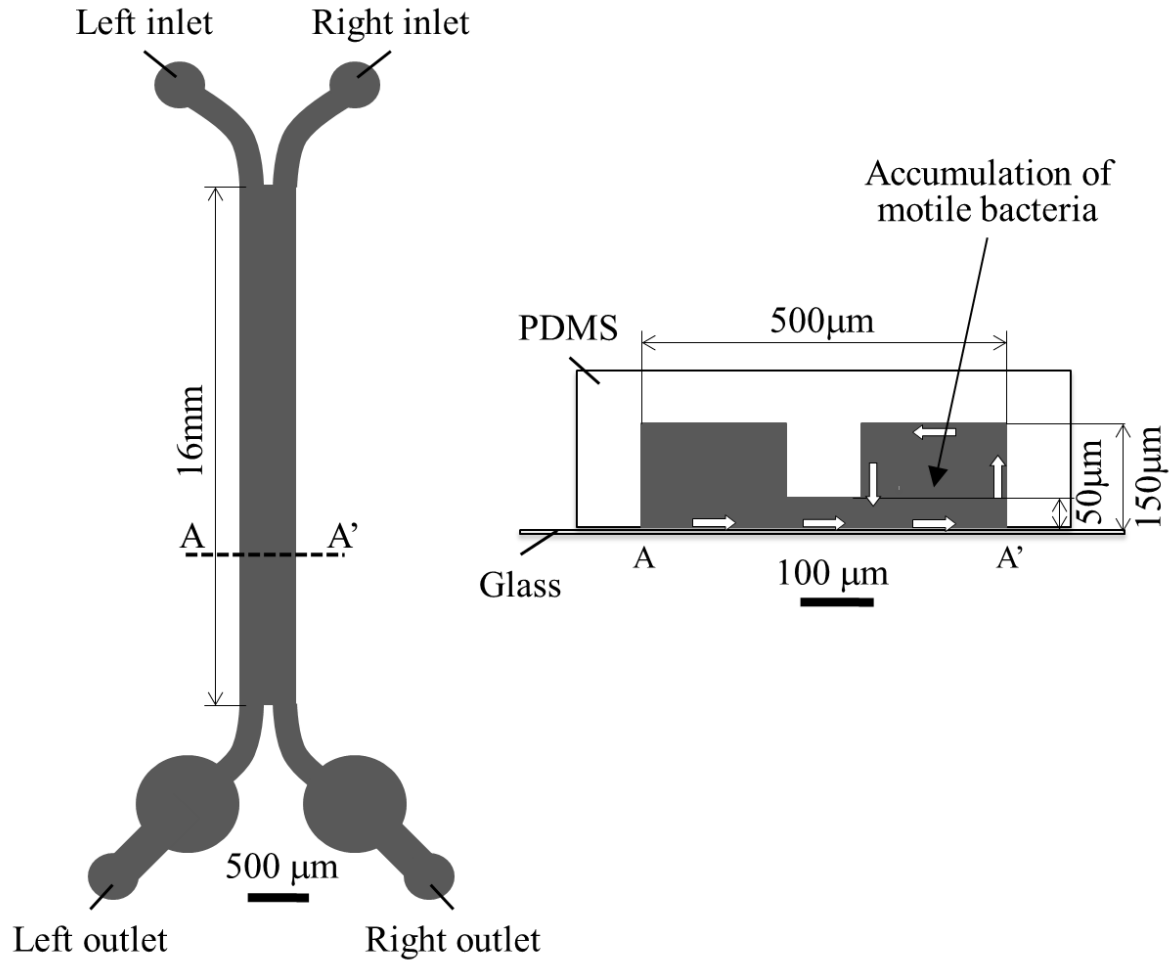

(a) Microchannel A: The main channel was 500 μm wide, 16 mm long, and either 50 or 150 μm high.

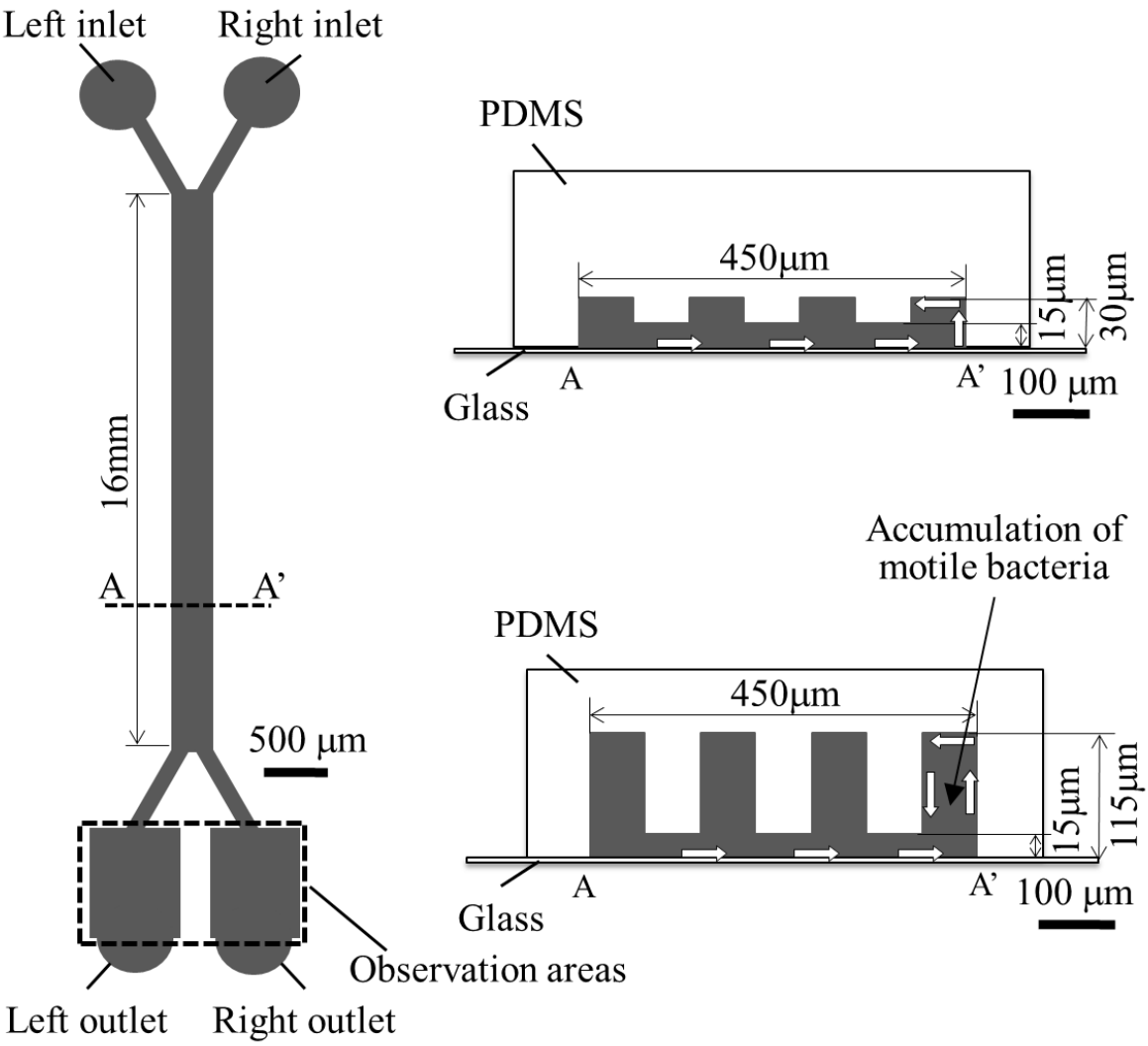

(b) Microchannel B: The main channel was 450 μm wide and 16 mm long. The minimum height of the channel was 15 μm, and the maximum height *H* was 30 or 115 μm.

Figure 1: Schematic representations of PDMS microchannel A for observing drift phenomena and microchannel B for separating motile bacteria. White arrows indicate the behavior of motile bacteria; motile cells are accumulated on the right side.

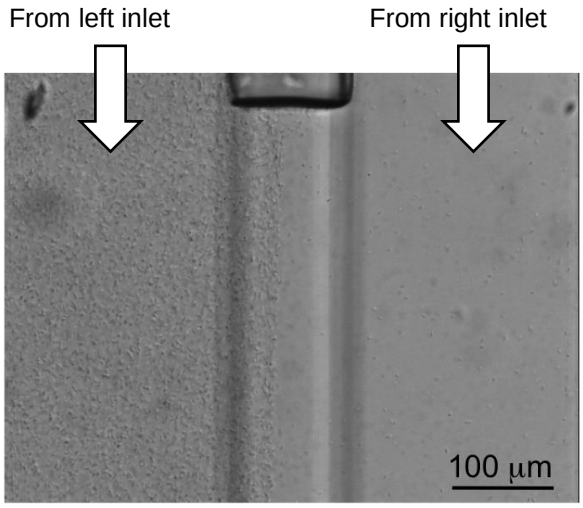

(a) near the entrance (motile cells)

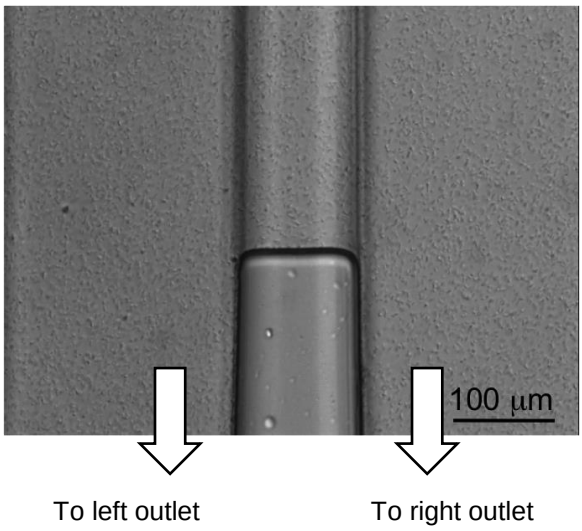

(b) near the exit (motile cells)

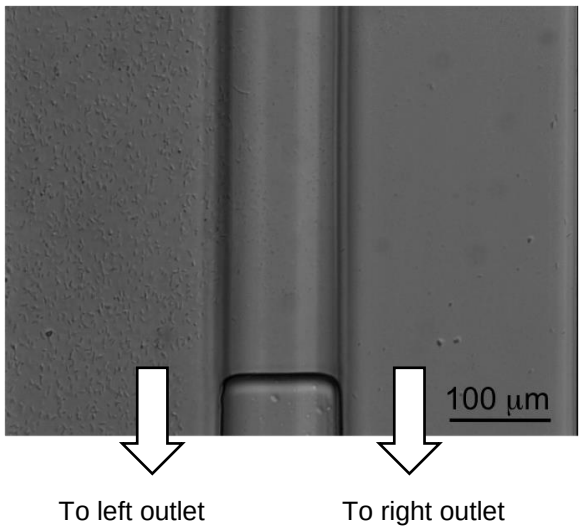

(c) near the exit (non-motile cells)

Figure 2: Distribution of motile or non-motile *E. coli* near the entrance or the exit of the main channel at a flow rate of 1.2 μL/min (Microchannel A). Cell culture [nmotile MG1655 or non-motile MG1655] was introduced via the left inlet, and TB was introduced via the right inlet. The flow rates at the left and right inlets and the left and right outlets were identical.

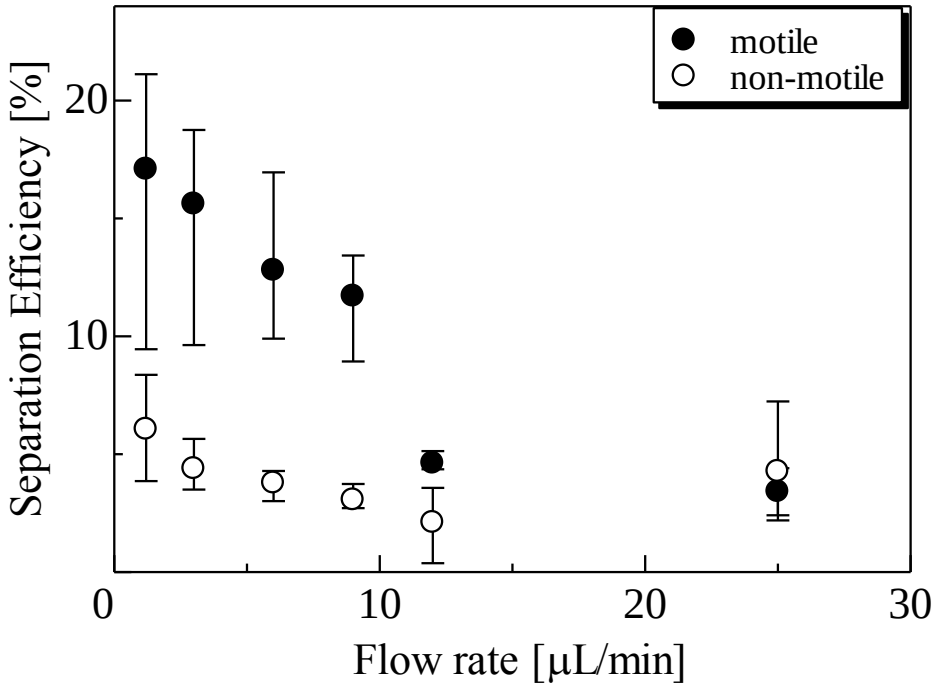

Figure 3: Separation efficiencies of motile and non-motile bacteria as a function of flow rate (microchannel A). The error bars indicate the range of three independent experiments.

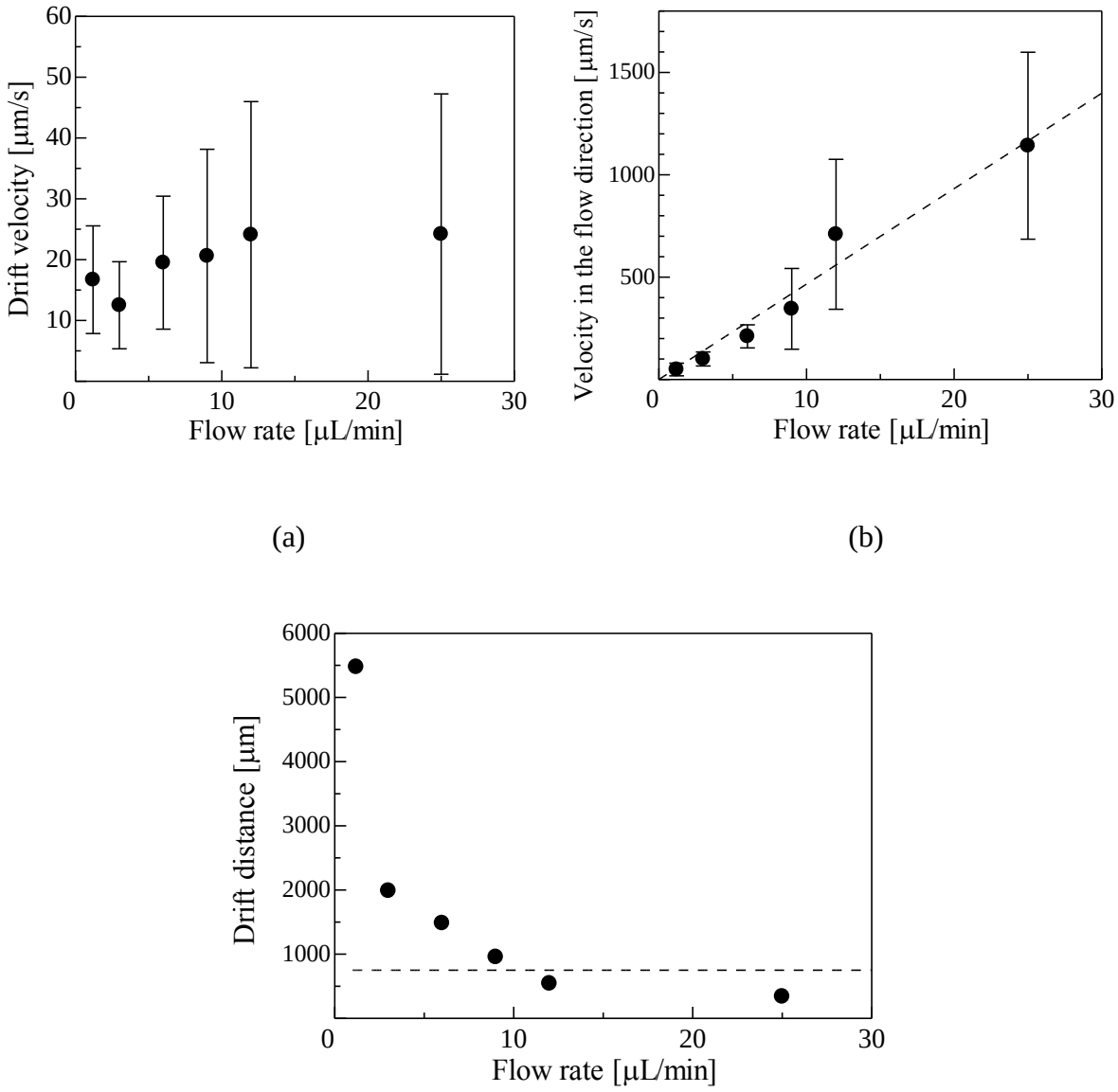

Figure 4: Drift phenomena in microchannel A: (a) drift velocity, or the velocity towards the right side, as a function of flow rate (The error bars indicate the standard deviation of about 20 cells), (b) velocity in the flow direction as a function of flow rate (The error bars indicate the standard deviation of about 20 cells), where the broken line is fitted by the method of least squares, and (c) drift distance calculated from the drift velocity, velocity in the flow direction, and a channel length of 16 mm. The broken line indicates the half length of the wetted perimeter.

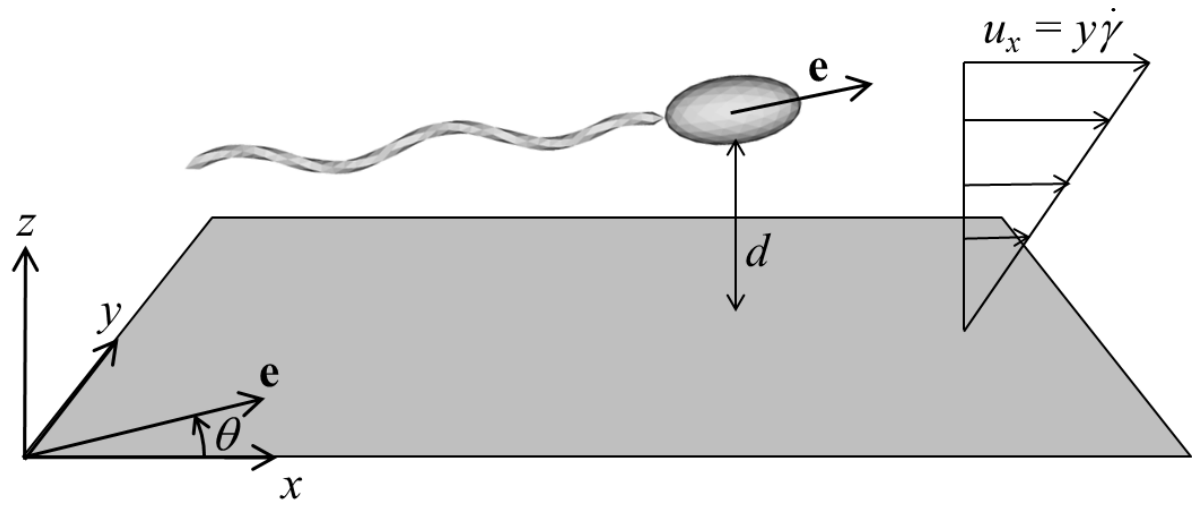

Figure 5: Computational setup for a boundary element analysis. A wall boundary existed at $z = 0$. x was taken in the flow direction, and y was taken in the lateral direction. The background flow was assumed to be $\mathbf{u} = (\dot{\gamma} z, 0, 0)$, i.e. simple shear flow. Vector **e** was the unit orientation vector of a bacterium, and θ was the angle of vector **e** from the x axis in the x-y plane. Value d was the minimum distance between the wall and the cell body.

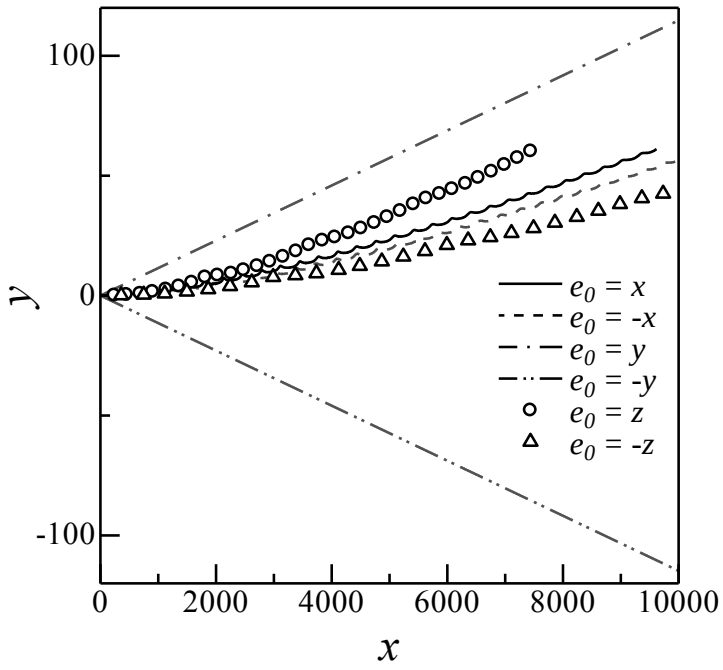

(a)

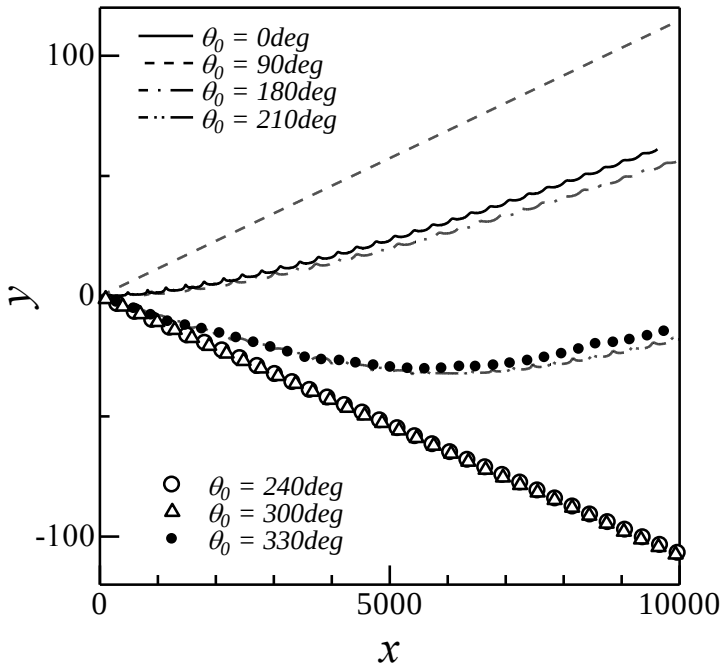

(b)

Figure 6: Trajectories of a bacterium in free space; *i.e.*, without a wall, at a shear rate of $\dot{\gamma} = 0.1\omega$: (a) initial orientation vector $\mathbf{e}_0$ as directed to each coordinate axis, and (b) $\mathbf{e}_0$ was in the *x*-*y* plane, and the initial orientation angle θ_0 was varied.

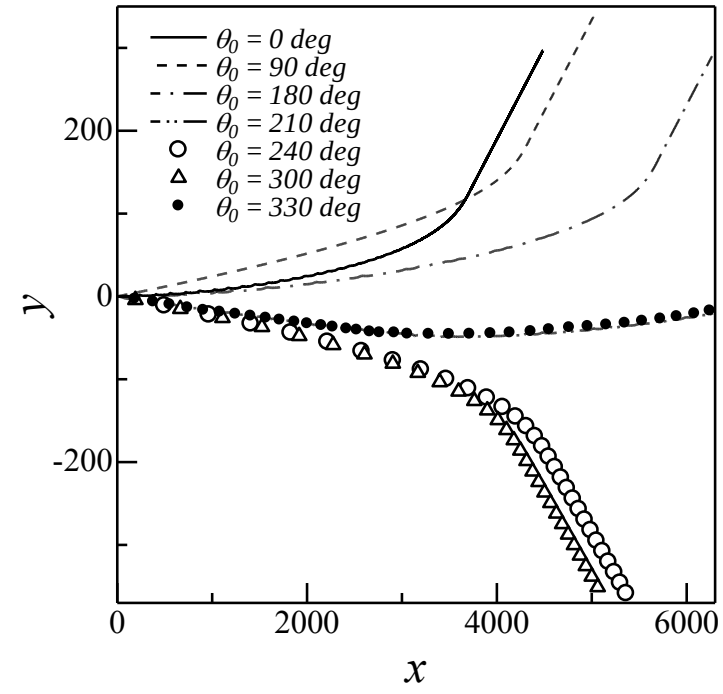

(a)

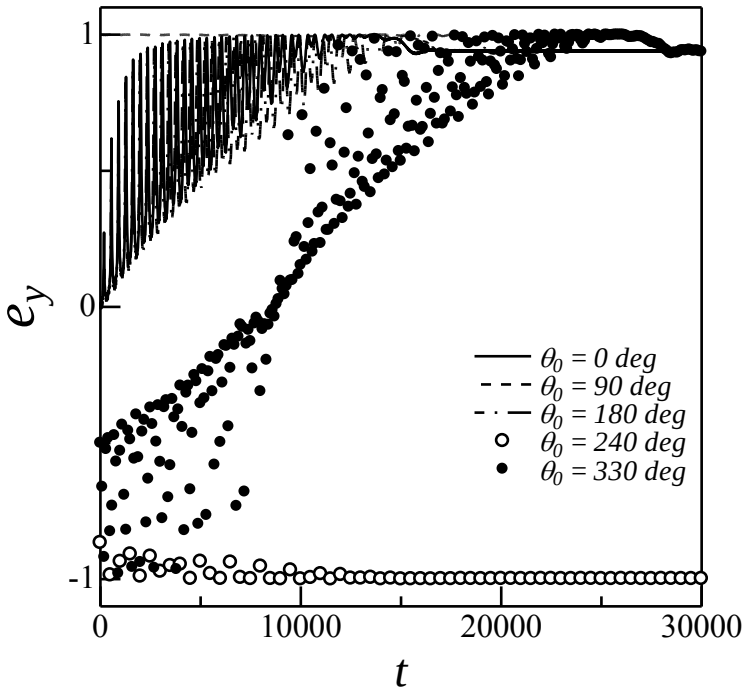

(b)

Figure 7: Swimming motion of a bacterium in shear flow near a wall ($\dot{\gamma} = 0.1\omega$). The initial distance d_0 was 4.5a, and the initial orientation angle θ_0 was varied while keeping $\mathbf{e}_0$ in the x-y plane: (a) trajectories, and (b) y component of the orientation vector e_y as a function of time t.

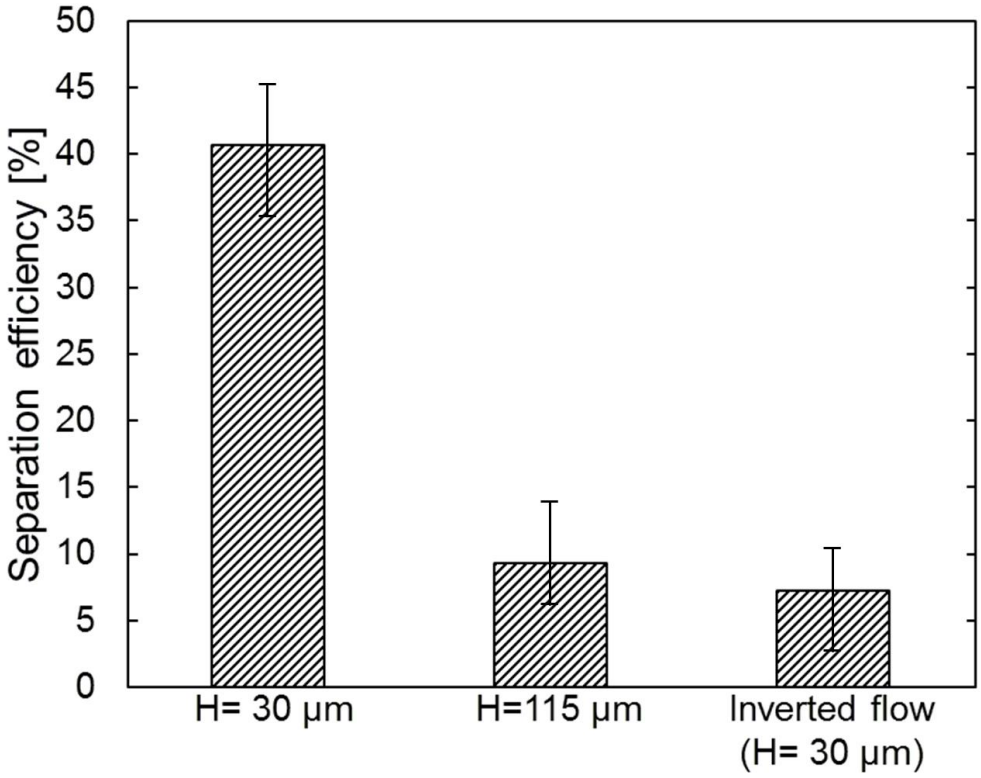

Figure 8: Separation efficiency of bacteria from fluorescence tracer particles using microchannel B. Value *H* was the maximum height of the channel, and 'Inverted flow' indicates that the bacterial suspension was injected via the right inlet. The error bars indicate the range of three independent experiments.

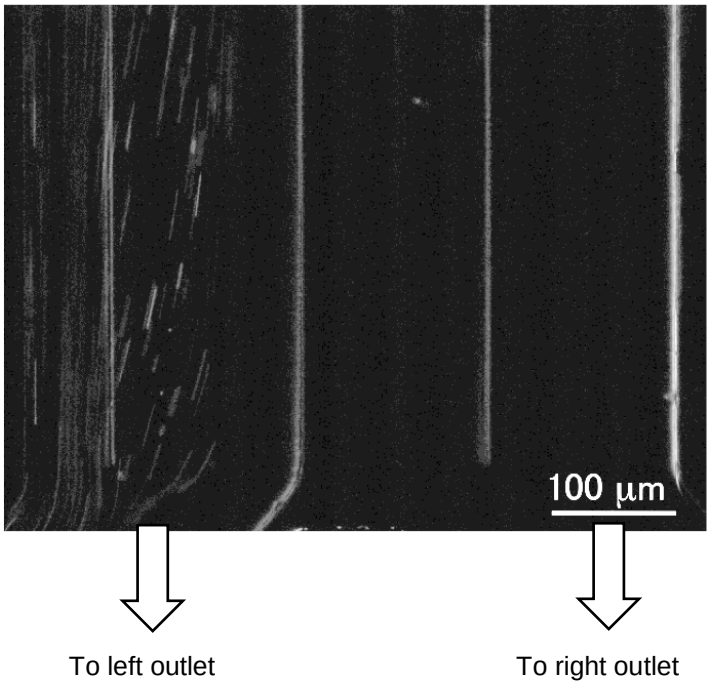

(a)

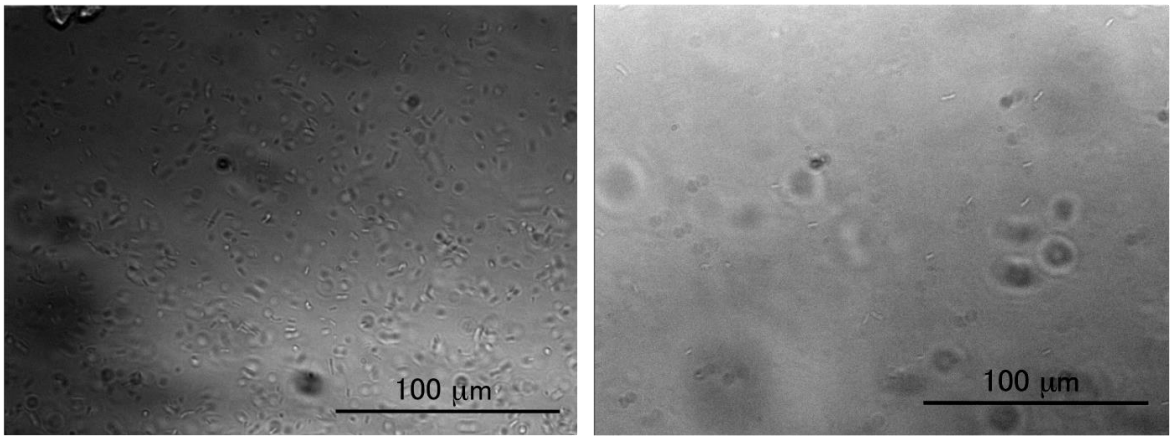

(b) (c)

Figure 9: Motion of less-motile and motile bacteria in microchannel B: (a) fluorescence image showing labeled less-motile bacteria (JK109) near the left outlet, (b) bright-field image of the left outlet, and (c) bright-field image of the right outlet.

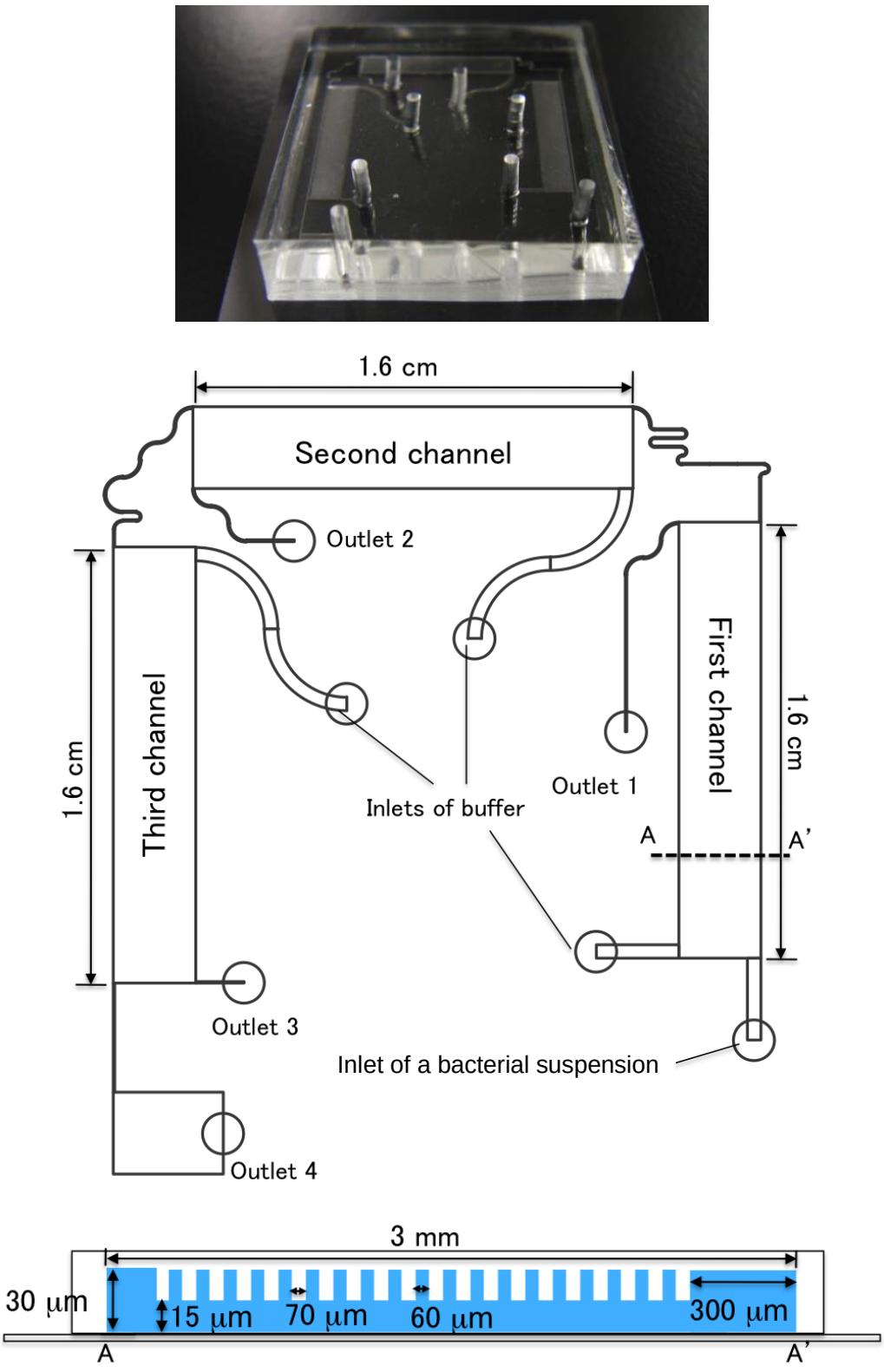

Figure 10: A schematic representation of a series of three PDMS microchannels, which has one inlet of a bacterial suspension, three inlets of buffer fluid and four outlets. The cross section in the A-A' plane is shown at the bottom. Outlook of the device is shown on top.